

# New experiments with a double crystal electron interferometer<sup>★</sup>

Amir H. Tavabi<sup>1</sup>, Martial Duchamp<sup>1,2,a</sup>, Vincenzo Grillo<sup>3,4</sup>, Rafal E. Dunin-Borkowski<sup>1</sup>, and Giulio Pozzi<sup>1,5</sup>

<sup>1</sup> Ernst Ruska-Centre for Microscopy and Spectroscopy with Electrons (ER-C) and Peter Grünberg Institute (PGI), Forschungszentrum Jülich, 52425 Jülich, Germany

<sup>2</sup> School of Materials Science and Engineering, Nanyang Technological University, 50 Nanyang Avenue, 639798 Singapore

<sup>3</sup> CNR-Institute of Nanoscience-S3, Via G. Campi 213/a, 41125 Modena, Italy

<sup>4</sup> CNR-IMEM, Parco delle Scienze 37a, 43100 Parma, Italy

<sup>5</sup> Department of Physics and Astronomy, University of Bologna, Viale B. Pichat 6/2, 40127 Bologna, Italy

Received: 21 October 2016 / Received in final form: 2 February 2017 / Accepted: 29 March 2017  
© EDP Sciences 2017

**Abstract.** Recent advances in transmission electron microscopy and specimen preparation now permit the revival of an old idea, originally pioneered by Marton, of using single crystals as amplitude division beam splitters. As a first step in the direction of realizing a three crystal electron interferometer, we present results obtained from a double crystal interferometer, in which the gap between the two crystals is under experimental control and perfect registry is obtained by using focused ion beam milling to fabricate the interferometer from a single Si crystal.

## 1 Introduction

In 1977, Rackham and co-workers observed remarkable and unusual interference phenomena in a transmission electron microscope (TEM) from a diffracting object that consisted of two perfectly aligned, simultaneously diffracting crystals that were separated by a gap in the electron beam direction [1]. They were able to interpret the main features of the diffraction patterns [2] and reported that they could obtain such double crystals routinely by ion bombardment. However, their specimen preparation method did not allow the gap between the crystals to be controlled and the maximum gap that they achieved was on the order of 1–2  $\mu\text{m}$ . Although they predicted that a double crystal interferometer (DCI) with a larger gap of approximately 10  $\mu\text{m}$  could be useful for holographic electron microscopy, this idea was not pursued. A subsequent realization of a DCI was achieved using voids in spinel [3], again with a spacing between the crystals of below 1  $\mu\text{m}$ .

In 1995, Zhou and co-workers [4] obtained new results by combining a Si DCI with convergent beam electron diffraction (CBED), taking advantage of a special structure formed at the broken edge of a Si [111] crystal. The gap between the crystals was still on the order of 1  $\mu\text{m}$  or below. They provided a theoretical interpretation of their results for a two beam orientation [5] and pointed out the possibility of extending the principle of holography to Fourier space [6].

<sup>a</sup> e-mail: mduchamp@ntu.edu.sg

<sup>★</sup>Contribution to the topical issue “The 16th European Microscopy Congress (EMC 2016)”, edited by Richard Brydson and Pascale Bayle-Guillemaud

These pioneering experiments were made with the purpose of using the device primarily for the measurement of lattice parameters (either by using one of the crystals as a specimen of interest or by inserting a specimen between the two crystals) [1]. However, it was also noted that the presence of interference effects in reciprocal space opened the way to performing holography in the Fraunhofer plane and obtaining information about the positions of atoms and the symmetry of the unit cell from the phases and amplitudes of the diffracted beams [5,6].

Unfortunately, as a result of the status of specimen preparation techniques at the time, these goals were not achieved. Today, the use of focused ion beam (FIB) milling for specimen preparation allows double crystal interferometers to be fabricated with the distance between the crystals under experimental control.

Here, we present results obtained from two DCIs that have different gaps of up to 8  $\mu\text{m}$  and are fabricated from a bulk Si single crystal using FIB milling. We show how such a setup can be used to provide better control over results that were previously obtained by chance [7]. The preservation of spatial lattice coherence between such crystal slabs has been demonstrated previously in both X-ray and neutron interferometry [8–10].

This paper is organised as follows. In Section 2, the principle of the method is reviewed. Section 3 briefly describes the experimental approach that is used for specimen preparation (by FIB milling) and the theoretical interpretation of the experimental results (by means of multislice calculations). Section 4 contains results obtained using smaller gaps, which can be compared directly with results obtained by previous authors and

are interpreted using the multislice method. Section 5 is then dedicated to results obtained using larger gaps that are particularly useful for holography applications and describes a first, partially successful, attempt to build a three-crystal Mach-Zehnder interferometer according to Marton's proposal [11–13].

## 2 Basic principle

When a convergent electron beam illuminates the upper crystal in a DCI (Fig. 1), the direct and diffracted beams are separated by a distance that depends on the orientation of the crystal. For the sake of simplicity, let us initially assume that only one reflection  $g = 1/d$  is excited. The two beams propagate between the crystals, which are separated by a distance  $D$ . At the second crystal, they diffract again to form four partial waves. Of these four beams, two continue in the direction of the direct electron beam, while the other two continue in the direction of the diffracted beam.

In the far-field region, i.e., in the Fraunhofer plane, the parallel waves overlap and their interference results in a system of sinusoidal fringes that are aligned perpendicular to the direction of the  $g = 1/d$  reflection. In practice, the final recording plane is conjugate to the back focal plane of the objective lens. By considering two virtual sources that are separated by  $gD\lambda$  (where  $\lambda$  is the de Broglie wavelength) in a microscope with camera length  $L$ , a hologram with fringe spacing  $\Delta = Ld/D$  is formed within the discs. It should be noted that the fringe spacing in the hologram is independent of the electron wavelength. This simple geometrical description can be improved by taking into account kinematical and dynamical effects [2, 5].

## 3 Experimental and theoretical methods

An FEI Helios dual beam FIB workstation equipped with an in situ micro-manipulator, a Pt gas injector system and an alpha flip stage was used to fabricate a DCI. A Pt layer was deposited in situ in the FIB prior to the extraction of a  $15 \times 4 \times 5 \mu\text{m}$  lamella from a Si (100) wafer. The lamella was transferred to an OmniProbe grid inside the FIB using a standard lift-out procedure [14, 15]. Thinning of the lamella and milling of the trenches was performed with a 30 kV Ga ion beam using currents of 0.28 nA and 93 pA, respectively. In order to minimise surface damage, a 5 kV cleaning step was performed. Great care was taken to minimise implantation of  $\text{Ga}^{2+}$  ions by keeping the number of FIB snapshots as low as possible and by not irradiating the lamella directly [16].

Two different specimens were fabricated. In the first specimen, the gap distances  $D$  were 200, 400, 600 and 800 nm and the films were prepared so that, for each gap, single crystal and double crystal cases could be compared. It is possible to image the transition from a single crystal to a double crystal by placing a convergent electron beam

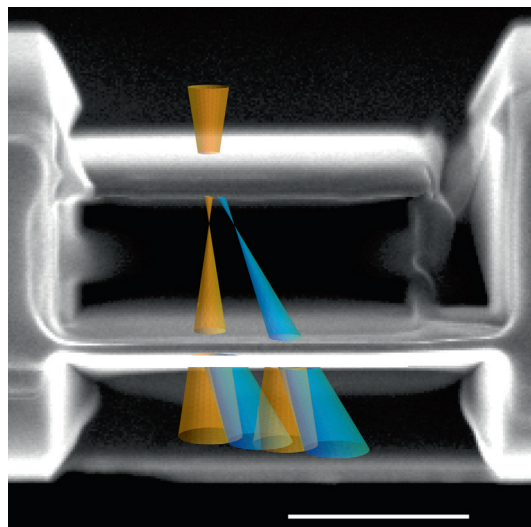


**Fig. 1.** Scanning electron micrograph showing two Si crystals separated by a distance  $D = 800$  nm. Superimposed on the image is a sketch of the ray path of a convergent beam that describes the generation of a transmitted beam and a diffracted beam by the upper crystal. These beams, in turn, impinge on the lower crystal and generate further transmitted and diffracted beams that overlap and interfere in the Fraunhofer diffraction plane. Scale bar:  $1 \mu\text{m}$ .

at the edge of the top crystal, so that half of it passes through the first crystal and half of it remains in vacuum. In this way, the half of the beam that is unaffected by the first crystal travels to the second crystal and produces a standard convergent beam diffraction pattern (containing no interference fringes), while the other half of the beam travels through both crystals and produces multiple interference fringes, as the crystal is close to a zone axis orientation.

This situation is shown in Figure 2, in which the upper right part of each spot shows interference fringes that are associated with overlap of the two crystals, whereas they are absent in the lower left part of each spot, which corresponds to intensity recorded from only one crystal.

In order to interpret the results shown in Figure 2, as well as those obtained when only a systematic row of reflections is excited, we performed multislice simulations of interference patterns using a combination of STEM.CELL [17] and Kirkland [18] software. The calculations were carried out for two conditions: first for two slabs of Si [110], each 100 nm thick, with a variable separation between them and second for a systematic row orientation with a strong excitation of  $\{111\}$  reflections. The accelerating voltage was 200 kV, as in the experiments, while the incident electron beam convergence semi-angle was varied between 2 and 3 mrad to match the experiments. In detail, a probe was generated with an overfocus  $f$  equal to half the separation between the two Si slabs. A dynamical calculation was performed for propagation in the first slab. The exit wave after the first slab was propagated freely using a numerically evaluated Fresnel

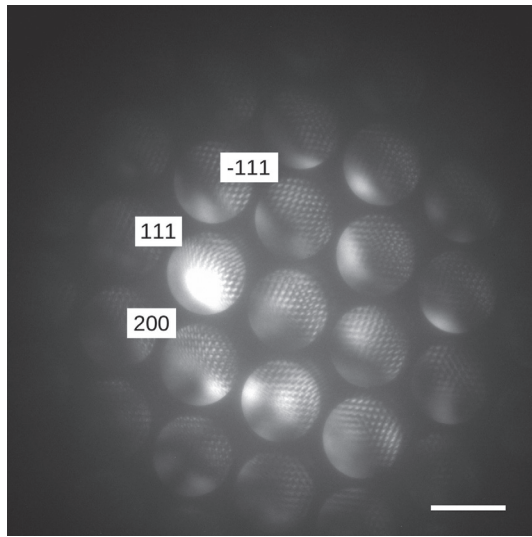


**Fig. 2.** Convergent beam electron diffraction pattern showing a transition between single Si crystal and double Si crystal interference phenomena. Scale bar:  $2 \text{ nm}^{-1}$ .

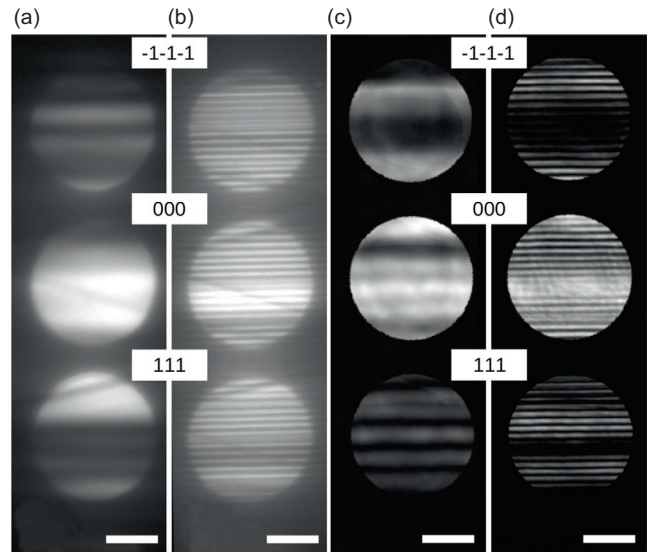
integral to the second slab. A second multislice calculation was then performed and the wavefunction after the second slab was finally Fourier transformed to calculate the intensity of the recorded CBED pattern. The two multislice simulations were carried out using the frozen lattice approximation for a single lattice configuration. Qualitatively, this has the effect of producing an uneven diffuse scattering background. Partial coherence was not included directly in the simulations. It can often be neglected in conventional CBED when no disks overlap. However, in the present case it may have an effect on the fringe visibility.

#### 4 Experimental results for a small gap

Experiments were carried out in a CM20 FEG TEM operated at 200 kV using a double tilt specimen holder. Either 70 or 100  $\mu\text{m}$  condenser apertures were used, depending on the diffraction conditions, in order to avoid overlap between the convergent beams. Exposure times were 0.2 s for the single crystal and 0.5 s for the overlapped crystals.

Figure 3 shows a typical diffraction pattern recorded in the Fraunhofer plane for a separation between the Si crystals of  $D = 800 \text{ nm}$  and a near-two-beam orientation. Figure 3a shows spots that have been diffracted only by the second crystal (on the right side of Fig. 1). Figure 3b shows a diffraction pattern recorded after the beams had travelled through both crystals, with the interference fringes clearly visible. Corresponding simulations are shown in Figures 3c and 3d, respectively. The match between the experimental results and the simulations is convincing and confirms that the sample quality is good enough not to introduce artifacts.

The use of a DCI near a zone axis orientation leads to more impressive results, as shown in Figure 2.



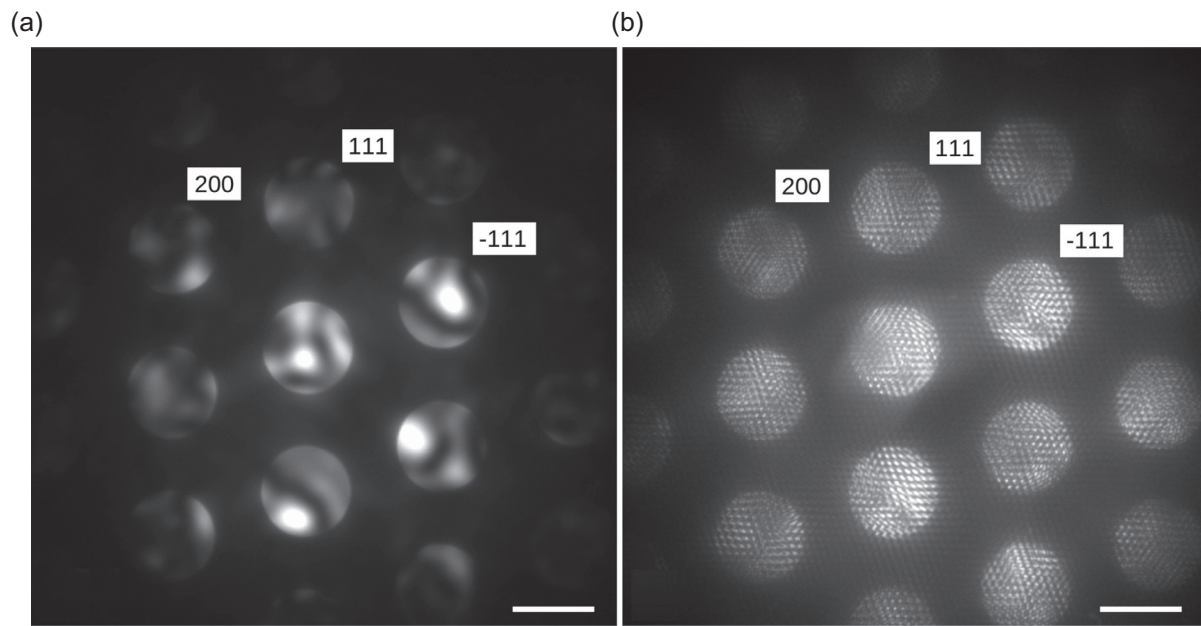
**Fig. 3.** Convergent beam electron diffraction patterns recorded from (a) a single Si crystal and (b) two overlapping crystals in a two beam orientation. Interference fringes are clearly visible in (b). The spacing between the crystals is  $D = 800 \text{ nm}$ . (c, d) Multislice simulations of diffraction patterns of a single crystal and two overlapping crystals, respectively. Scale bar:  $2 \text{ nm}^{-1}$ .

Figure 4 shows a comparison of a standard CBED pattern recorded from a single crystal in Figure 4a with a complicated system of interference fringes arising from the overlap of many diffracted beams in Figure 4b. As in any interference phenomenon, such a pattern encodes the phase difference between the interfering beams, which is primarily of crystallographic origin in this case. The interference fringe spacing is inversely proportional to the separation of the crystals  $D$  in each individual diffraction direction.

Figure 5 shows a multislice simulation of the former result. Dynamical diffraction was included in the simulation, but no attempt was made to match the exact diffracting condition.

#### 5 Experimental results for large gaps

As mentioned above, the fringe spacing is inversely proportional to the separation of the crystals  $D$ . However, our experiments and simulations show additional modulations in the positions and intensities of the fringes due to dynamical scattering. We fabricated a second DCI that had separations between the crystals of 2, 4 and 8  $\mu\text{m}$ , as shown in Figure 6. The top view SEM image of the specimen shows on the left two crystals separated by 2  $\mu\text{m}$ , which were used mainly for selecting the diffracting conditions. The center part shows three overlapped crystals separated by  $D = 4 \mu\text{m}$ , which were fabricated to allow the diffracting conditions to be selected with a gap of  $D = 4 \mu\text{m}$  on the left and  $D = 8 \mu\text{m}$  on the right,



**Fig. 4.** Comparison of diffraction patterns recorded from (a) a single Si crystal and (b) two overlapping crystals in a zone axis orientation. The spacing between the crystals is  $D = 800$  nm. Scale bar:  $2 \text{ nm}^{-1}$ .

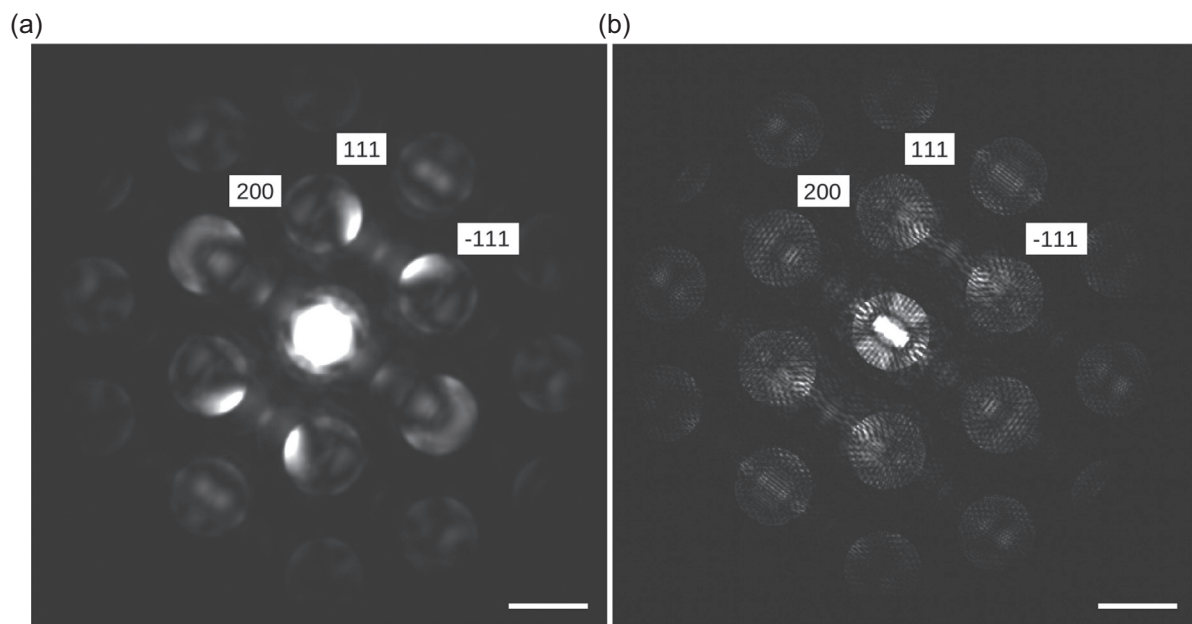


**Fig. 5.** Multislice simulation of interference fringes generated by two overlapping Si crystals separated by a distance  $D = 800$  nm at a zone axis orientation for (a) a single Si crystal and (b) two overlapping crystals. Scale bar:  $2 \text{ nm}^{-1}$ .

whereas in the center is our first attempt at fabricating a Mach-Zehnder interferometer.

Experiments were carried out in a Tecnai G2 F20 FEG TEM operated at 200 kV using a double tilt specimen holder. In order to detect very fine fringes, the experiments were carried out at the largest available camera length of 3 m using exposure times of 1–2 s. Alternatively, a smaller nominal camera length could be used, with additional magnification provided by using the camera of the energy filter. The energy filter was also found to be useful

to enhance the fringe contrast for the  $2 \mu\text{m}$  gap, owing to the thickness of the crystals.

In Figures 7 and 8, we present results obtained for gaps of 4 and 8  $\mu\text{m}$ , respectively, with the crystal at a strong systematic row orientation, at which clear closely-spaced interference fringes are visible. The higher magnification inset shows additional modulations arising from other excited beams.

Unfortunately, the experiments that were carried out using the three-crystal interferometer were not successful,

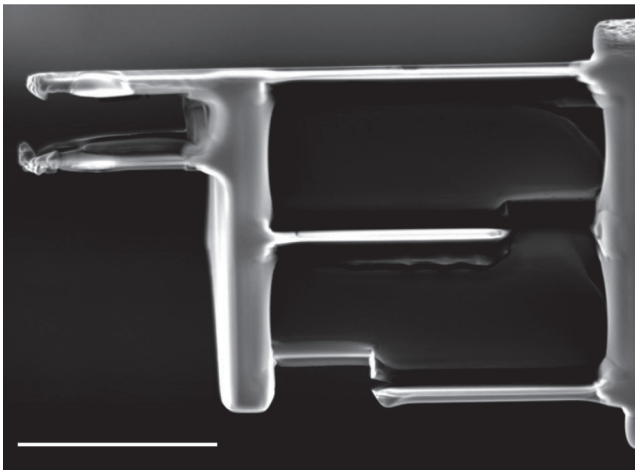


**Fig. 6.** Top view of a specimen with larger gaps. On the left, the two crystals are separated by  $2\ \mu\text{m}$ . On the right, three crystals are separated by  $4\ \mu\text{m}$ , with holes that allow the observation of interference patterns with a gap of  $4\ \mu\text{m}$  on the left and  $8\ \mu\text{m}$  on the right, whereas at the centre a three-crystal setup is present. Scale bar:  $5\ \mu\text{m}$ .

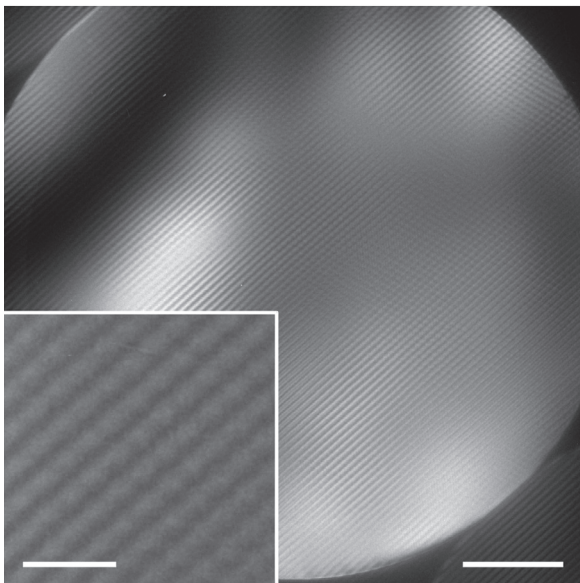


**Fig. 7.** Convergent beam electron diffraction pattern recorded from two Si crystals separated by a distance  $D = 4\ \mu\text{m}$ . Scale bar:  $0.5\ \text{nm}^{-1}$ . The inset (scale bar:  $0.1\ \text{nm}^{-1}$ ) shows the interference fringes at higher magnification.

primarily because the relatively small distance between the crystals made it impossible to use the standard microscope apertures to extract a ray path corresponding to the Mach-Zehnder setup. In X-ray [8,9] or neutron [10] interferometry, the functioning of a Mach-Zehnder setup can be confirmed by inserting a variable phase shifter into one of the arms of the interferometer. Its absence in our experiment makes the results difficult to interpret. However, the presence of the expected interference fringes at larger spacings confirms that coherence is well preserved.

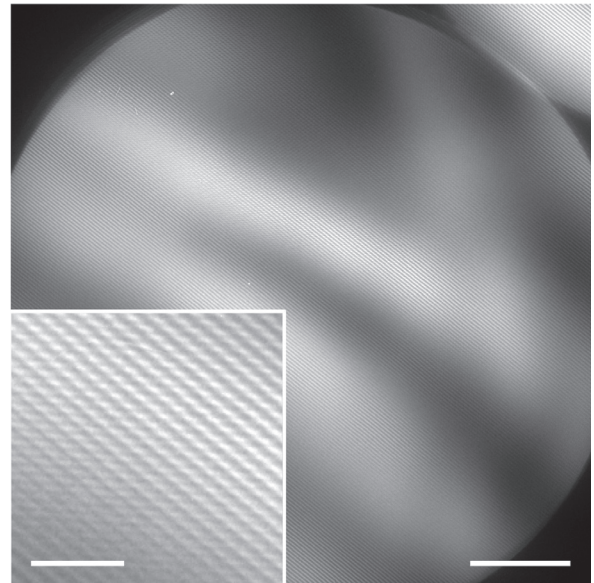


**Fig. 8.** Convergent beam electron diffraction pattern recorded from two Si crystals separated by a distance  $D = 8\ \mu\text{m}$ . Scale bar:  $0.5\ \text{nm}^{-1}$ . The inset (scale bar:  $0.1\ \text{nm}^{-1}$ ) shows the interference fringes at higher magnification.

## 6 Conclusions

In conclusion, we have shown that it is possible use FIB milling to fabricate DCIs, in which the gap distances are under experimental control and are as large as  $8\ \mu\text{m}$  in our experiments. Our results pave the way for the realisation of proposals envisaged in early pioneering papers [1,5,6], as well as opening new perspectives for the field of electron interferometry and holography.

Our experiments demonstrate the fact that changes in specimen thickness can introduce variations across the illuminated area, as well as the need for better control of the diffracting conditions. Once these problems are solved, the lack of versatility of the DCI (as the fringe spacing depends on the gap distance and the diffracting conditions) will be largely compensated by the more relaxed spatial coherence requirements and the lack of Fresnel diffraction resulting from the sharp edges of an electron biprism wire. If a specimen is inserted between the crystals, either by depositing it onto the lower crystal or by placing it in a conjugate plane in the electron microscope, then it will be possible to obtain Fresnel or Fourier off-axis electron holograms with an exposure time as low as  $0.05\ \text{s}$ , i.e., two orders of magnitude below the exposure times of standard electron holograms obtained using an electron biprism (typically a few seconds).

Our experiments also show that the time is ripe for the re-introduction into electron microscopy of the Marton three crystal interferometer [11–13] if the gap between the crystals can be increased to a value that allows the selection of a Mach-Zehnder ray path using standard microscope apertures. Work is in progress in this direction, as such a device could also be used to

realize interaction-free measurement schemes, as recently proposed by Kruit and co-workers [19].

We are grateful to the European Union Seventh Framework Programme for funding under Grant Agreement 312483-ESTEEM2 (Integrated Infrastructure Initiative-I3). The research leading to these results has received funding from the European Research Council under the European Union's Seventh Framework Programme (FP7/2007-2013)/ ERC grant agreement number 320832. V.G. is very grateful for funding from the Alexander von Humboldt Foundation. The authors would particularly like to acknowledge the anonymous referees for their valuable comments on an earlier version of this paper.

## References

1. G.M. Rackham, J.E. Loveluck, J.W. Steeds, in *IoP Conference Series: Electron Diffraction 1927–1977*, edited by P.J. Dobson, J.P. Pendry, C.J. Humphreys (Institute of Physics Publishing, 1977), vol. 41, p. 435
2. B.F. Buxton, G.M. Rackham, J.W. Steeds, in *Proceedings of the Ninth International Congress on Electron Microscopy*, edited by J.M. Sturgess (Microscopical Society of Canada, Toronto, 1978), vol. 1, p. 188
3. B. DeCooman, C. Carter, *Ultramicroscopy* **13**, 233 (1984)
4. F. Zhou, E. Plies, G. Möllenstedt, *Optik* **98**, 95 (1995)
5. F. Zhou, *J. Electron Microsc.* **50**, 371 (2001)
6. F. Zhou, *Microsc. Microanal.* **9**, 64 (2003)
7. A.H. Tavabi, M. Duchamp, R.E. Dunin-Borkowski, G. Pozzi, in *Proceedings of the 16th European Microscopy Congress, Lyon, France* (The 16th European Microscopy Congress, Lyon, France, 2016), pp. 711-712
8. M. Hart, *Proc. Royal Soc. London A: Math. Phys. Sci.* **346**, 1 (1975)
9. V.V. Lider, *Physics-Uspekhi* **57**, 1099 (2014)
10. H. Rauch, S.A. Werner, *Neutron Interferometry: Lessons in Experimental Quantum Mechanics, Wave-particle Duality, and Entanglement* (Oxford University Press, 2015)
11. L. Marton, *Phys. Rev.* **85**, 1057 (1952)
12. L. Marton, J.A. Simpson, J.A. Suddeth, *Phys. Rev.* **90**, 490 (1953)
13. L. Marton, J.A. Simpson, J.A. Suddeth, *Rev. Sci. Instrum.* **25**, 1099 (1954)
14. L.A. Giannuzzi, J.L. Drown, S.R. Brown, R.B. Irwin, F.A. Stevie, in *Specimen Preparation for Transmission Electron Microscopy IV, MRS Symposium Proceedings*, edited by R.M. Anderson, S.D. Walck (Materials Research Society, Pittsburgh, PA, 1997), Vol. 480, p. 19
15. L.A. Giannuzzi, B. Kempshall, S. Schwarz, J. Lomness, B. Prenitzer, F. Stevie, in *Introduction to Focused Ion Beams*, edited by L.A. Giannuzzi (Springer, 2005), p. 201
16. M. Duchamp, Q. Xu, R.E. Dunin-Borkowski, *Microsc. Microanal.* **20**, 1638 (2014)
17. V. Grillo, E. Rotunno, *Ultramicroscopy* **125**, 97 (2013)
18. E.J. Kirkland, *Advanced Computing in Electron Microscopy* (Plenum Press, New York, 1998)
19. P. Kruit et al., *Ultramicroscopy* **164**, 31 (2016)